Heat deposition into the superconducting central column of a spherical tokamak fusion plant

C G Windsor[1], J G Morgan[2] and P F Buxton[1,3]

[1] Tokamak Energy, D5, Culham Science Centre, Abingdon, OX14 3DB

[2] Culham Electromagnetics, D5, Culham Science Centre, Abingdon, OX14 3DB

[3] York Plasma Institute, Department of Physics, University of York, Heslington, York, YO10 5DD

E-mail: `colin.windsor@virgin.net`

Abstract. A key challenge in designing a fusion power plant is to manage the heat deposition into the central core containing superconducting toroidal field coils. Spherical tokamaks have limited space for shielding the central core from fast neutrons produced by fusion and the resulting gamma rays. This paper reports a series of 3-dimensional computations using the Monte Carlo N-Particle (MCNP) code to calculate the heat deposition into the superconducting core. For a given fusion power, this is considered as a function of plasma major radius R_0, core radius r_{sc} and shield thickness d. Computations over the ranges $0.6\,\mathrm{m} \le R_0 \le 1.6\,\mathrm{m}$, $0.15\,\mathrm{m} \le r_{sc} \le 0.25\,\mathrm{m}$ and $0.15\,\mathrm{m} \le d \le 0.4\,\mathrm{m}$ are presented. The deposited power shows an exponential dependence on all three variables to within around 2%. The additional effects of source profile, the outer shield and shield material are all considered. The results can be interpolated to 2% accuracy and have been successfully incorporated into a system code. A possible pilot plant with 174 MW of fusion is shown to lead to a heat deposition into the superconducting core of order 30 kW. An estimate of 1.7 MW is made for the cryogenic plant power necessary for heat removal, and of 88 seconds running time for an adiabatic experiment where the heat deposition is absorbed by a 10 K temperature rise.

PACS numbers: 52.55.Fa, 28.52.Av, 84.71.Ba

Submitted to: *Nuclear Fusion*

1. Introduction

Calculations now suggest that by using the high plasma pressures possible with spherical tokamaks and the high magnetic fields possible with high temperature superconducting coils, it may be possible to construct a relatively compact fusion power plant [1, 2]. A key problem for this approach has been the heat deposition from fusion neutrons into a superconducting core. Algebraic estimates of this heating power have been made by Stambaugh *et al* [3]. For the Vulcan project Hartwig *et al* [4] also used the MCNP code but calculated the power deposition into the superconducting core as a function of shield

thickness at a fixed core and plasma radius. A detailed discussion of the inboard shield of ARIES-ST, with a conventional, central column, is given by El-Guebaly *et al* [5]. Their choice of a copper conductor was influenced by the cooling and shielding requirements of a conventional, low-temperature superconducting alternative. In contrast, the cryoplant requirements for a high-temperature superconducting central column, operating at 20 K rather than 4 K, are much less severe and we show that adequate shielding can be provided without compromising the low aspect ratio of a spherical tokamak design. The inboard shield must avoid any radial or other gaps that would allow neutron and gamma streaming.

We adopt a step-wise approach here, focusing on the shielding requirements. Rather than making all computations at the full level of detail, the complications are added in turn and their individual effects noted. For most of the computations the simplest practical model of a toroidal plasma at a major radius R_0 is taken with an elliptical cross section of minor radius a and elongation κ around a cylindrical superconducting core of radius $r_{\rm sc}$, surrounded by an annular shield of thickness d. Heat deposition into the superconducting core is presented over a wide range of these variables, and the results are discussed in geometric terms. The addition of an external shield at a radius $R_{\rm ext}$ and corresponding upper and lower shields at heights of $\pm Z_{\rm ext}$, is then considered and this is shown to increase the heat deposition by a small but significant contribution of order 6%. A further refinement is to define a radial profile of neutron production density described with a superposition of toroidal shells with differing elliptical cross-sections and differing power densities. This is shown to have heat deposition changes at a 20% level. Several potential shielding materials are considered. Tungsten carbide with water cooling was found to be the most promising on account of its high density and high atomic number, with the presence of low atomic number materials also providing neutron moderation. The results, corrected for the effects of the external shield and plasma profile are interpolated using least squares fitting into a form that can be incorporated into the plasma system codes used for power plant design such as that by Costley *et al* [2]. The particular example of a pilot plant with a major radius $R_0 = 1.35\,$m, a core radius $r_{\rm sc} = 0.23\,$m and a shield thickness $d = 0.37\,$m, similar to that considered by Costley *et al* will be considered throughout this study. It differs from the design reported by Costley *et al* by neglecting engineering features such a 0.05 m radius central tie-bar, a 0.03 m thermal shield insulation gap and a 0.05 m plasma-wall gap. MCNP computations show the inclusion of these particular features increases the heat deposition by some 89% over the simplified model. This significant increase results principally from the reduction in the thickness of the neutron shield to make room for the thermal break and the tie-bar. Further work aims to study these and other engineering factors individually to reveal their relative magnitudes.

MCNP6.1 is the latest release of a general-purpose, continuous-energy, general-geometry Monte Carlo code for N particles [6, 7]. It is a radiation transport code designed to track many particle types over a broad range of energies. It is supplied with an extensive library of nuclear cross-sections, allowing the computation of nuclear

interactions of fast neutrons, gamma rays and other secondary particles with most naturally-occurring isotopes of common elements. Detailed isotopic compositions can be specified for all materials used in a model.

With a long history of use in fusion research and incorporating substantial validation efforts, MCNP is the standard fusion neutronics tool with the ability to calculate a number of important nuclear quantities, including nuclear heating, radiation dose and damage, and tritium breeding. The detailed design for an optimized spherical tokamak power plant has yet to be made. The present calculations were performed with an idealized model of such a plant, while still maintaining full three-dimensional geometry, but with the simplifying assumption of axisymmetry. Compared with a full model, the results are much faster to obtain, more flexible and appropriate for a design study where parameters are being swept. Following such an optimization, a more detailed computation would be made.

A more detailed design study would also need to consider several additional factors affected by the choice and thickness of the neutron shield material. Induction losses could occur within a thick conducting shield. Radiation damage to the high-temperature superconductor may depend on different factors from those for its heat deposition. Activation and decay-heat production after operations need to be considered. If tritium breeding is envisaged, even on the outer shield, then the neutron reflectivity of the inner shield needs to be considered.

A second function of the neutron shield is to reduce the neutron damage to the high-temperature superconducting material. This can also be studied using MCNP but is not considered here. Experimental studies [8] show that at moderate levels the damage to high temperature superconductors kept at 20 K is limited at typical neutron fluences.

2. The starting point: a simplified cylindrical model

The simplest realistic model of a tokamak power plant will have the following three components, as shown in figure 1:

(i) A central superconducting core of radius r_{sc} containing the superconducting tapes, their cooling channels and the strengthening materials needed to restrain the large magnetic forces produced. The width of this core is variable within the range from 0.15 m to 0.25 m, depending on the currents needed to produce the required magnetic fields. In these first computations no detailed design is assumed; instead a homogeneous idealization of coil material, cooling and strengthening material is defined. An example coil material consists of 52.5% Hastelloy C-276, 22.5% copper and 25% neon cooling liquid by volume. Liquid neon has a high refrigerating capacity compared with gaseous helium on a per unit volume basis. The average density of this homogenized material was computed at 6.98 gcm^{-3}.

(ii) An annular radiation shield of thickness d varying from 0.15 m to 0.3 m. Options for the shielding material are discussed in section 6 but tungsten carbide with water

cooling was the best investigated and is used in most of the computations. This is assumed to be in the form of concentric cylinders, separated by concentric layers of cooling water.

(iii) A neutron-producing plasma. The MCNP code allows toroidal sources of elliptical cross section to be defined and versions of such a source composed of a superposition of several such toroidal volumes with varying radii can describe a source profile of some complexity. This source representation will be discussed in section 5, where we show that a single small elliptical torus centred close to the magnetic axis produces over half the emitted neutrons and deposits power in the core within 1% of the weighted superposition of eight toroids of varying sizes describing a typical plasma profile.

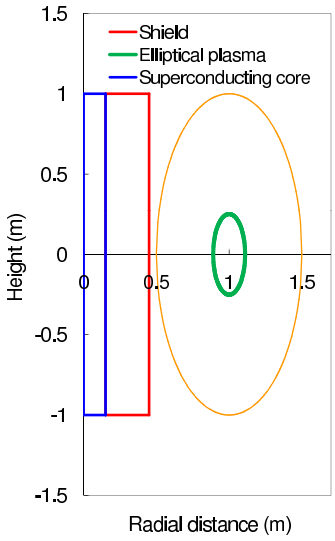

Figure 1. The simple toroidal model with 3-dimensional cylindrical geometry. The central core contains the high-temperature superconductors. It is surrounded by a cylindrical neutron shield. The toroidal plasma volume is assumed to produce neutrons uniformly within the central ellipse. The outer plasma boundary is also shown.

The calculations assume a surrounding cylindrical outer boundary of height ± 1.5 m and radius 1.6 m but no structural vessel or outer shielding. The purpose of this surface is to terminate the tracking of escaping particles that can have no further interaction with the structural components of the model. The effects of including a realistic outer shield over a rather larger outer boundary are considered in section 4.

The MCNP calculation proceeds by tracking the progress of some large number of fusion neutrons, typically around a million. These calculations take around 2 hours following 1.5 million particle histories. At each collision the possible reactions with the particular material are evaluated and outgoing particles followed. The objective is to capture fully the reactions that lead to nuclear heating from the source neutrons. This results in there being more neutrons to follow from *(n,2n)* reactions, and also many gamma rays to follow from the *(n,γ)* reactions. Typically the heating from gamma

rays is comparable with that from neutrons as found in the Vulcan studies [4]. As the numbers of neutrons and gamma rays decrease due to the shielding process, it is possible to improve the Monte Carlo statistics by increasing the number of tracked neutrons by artificially splitting them, and correspondingly reducing their weights, to give roughly similar neutron populations in each part of the material. The output from MCNP includes neutron and gamma ray mean free paths. In the shielding layer it is approximately 20 mm for neutrons, increasing to approximately 25 mm in the superconducting alloy core. Gamma ray mean free paths are about 25% shorter. The cylindrical core and annular shield have therefore been divided up into five radial sections with thicknesses of the order of these mean free paths. For example with a core radius $r_{\rm sc} = 0.15$ m, the radial steps are at 0.03, 0.06, 0.09, 0.12 and 0.15 m. With a shield thickness $d = 0.15$ m the five radial steps are at 0.18, 0.21, 0.24, 0.27 and 0.30 m. The program evaluates the statistical significance of all the computed output quantities ("tallies" in MCNP terminology), and these statistics are satisfactory for all the cases presented. The statistical accuracy of the MCNP computations is estimated in the output file to be of order 1%. A considerably larger error of order 10% must be expected on the overall reliability when the assumed simplifications of the geometry and plasma profile are taken into account.

A further separation has been made of the central core and shield into separate tally zones for their upper, central and lower parts, with the central zone being defined as ± 0.2 m from the mid-plane. This separation is to enable the heating to be determined in the peak mid-plane region of the core where the heating per unit length is expected to be a maximum.

The MCNP user may define energy bins to refine the information computed about the tallies. For the present computations twelve bins have been used, ranging from 0–1 keV up to 20–25 MeV; a few energetic particles are created in the latter range. Figure 2 shows the relative weights of the neutron and gamma heating contributions for each of these energy bands. It is seen that the neutrons have most weight in the energy range from 1 to 10 MeV. There is only a small contribution to the heat deposition from the energy range below 10 keV. The total heat deposition from neutrons and gammas is about the same for these parameters, however the neutron heating is more concentrated in the central mid-plane region.

3. The calculation of heat flow into the central core

A fusing plasma of say 174 MW total power emits some 139 MW as neutrons with the remainder as alpha particles. The alphas are slowed down within the plasma itself and their energy is mostly transported into the divertor region and partly transferred by relatively low energy radiation from the plasma onto the surface of the neutron shield and the remainder of the first wall. The alpha energy does not contribute significantly to the heat deposition into the body of the neutron shield or the superconducting core. We therefore consider only the heat deposition from the neutron production.

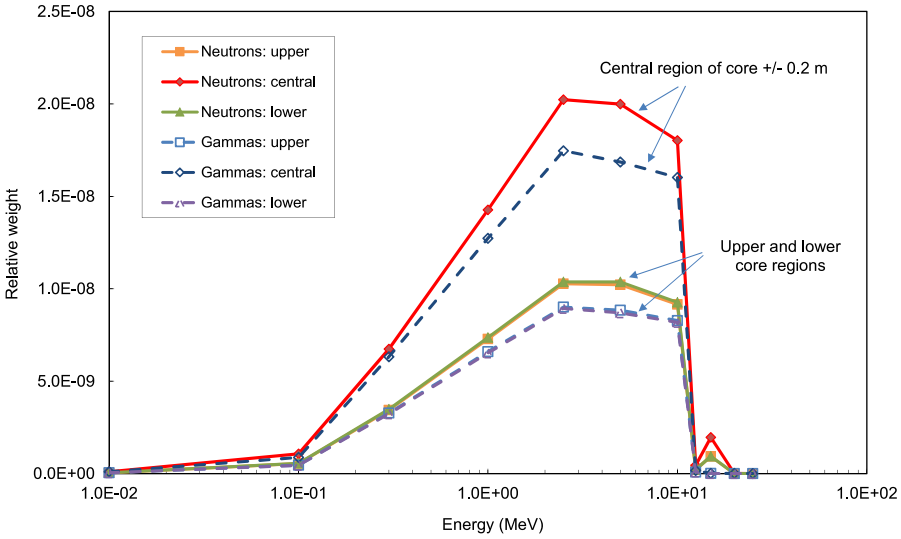

Figure 2. The relative weight of neutron and gamma power deposition as a function of energy on a log scale for a geometry with 0.15 m radius core and 0.15 m thickness shield. The relative weight is higher in the mid-plane zone closer to the centre of the source in both cases. Most of the heat arises from neutrons and gamma rays of relatively high energies above 100 keV.

The MCNP program produces an output file which contains both physics results and information about the Monte Carlo statistics. For example in the case of a core radius $r_{\rm sc} = 0.15$ m and shield thickness $d = 0.15$ m the energy deposited into the mid-plane $z = \pm 0.2$ m zone of the core region is $E_{\rm cc} = 6.40 \times 10^{-8}$ MeV per gram of this region per incident fusion neutron. Later in the output file the energy depositions into the upper zone $z > 0.2$ m, $E_{\rm uc}$ and into the lower zone $z < 0.2$ m, $E_{\rm lc}$ can be found. These three energies $E_{\rm cc}$, $E_{\rm uc}$ and $E_{\rm lc}$ and the corresponding masses $M_{\rm cc}$, $M_{\rm uc}$ and $M_{\rm lc}$ of the zones allow the calculation of the energy deposition into the complete superconducting core region. Each fusion neutron carries an energy from the D-T reaction of $E_{\rm DT} = 14.1$ MeV and if the total neutron power generated in the plasma is given by, for example: $P_{\rm neut} = 139$ MW then the total number of fusion neutrons produced per second will be $P_{\rm neut}/E_{\rm DT}$. The power deposition into the central region will therefore be $P_{\rm cc} = E_{\rm cc} M_{\rm cc} P_{\rm neut}/E_{\rm DT}$. Similarly for the complete core volume, the power deposition will be

$$P_{\rm tot} = (E_{\rm cc} M_{\rm cc} + E_{\rm uc} M_{\rm uc} + E_{\rm lc} M_{\rm lc}) P_{\rm neut}/E_{\rm DT} \ . \qquad (1)$$

These simple calculations are readily incorporated into a spreadsheet or the code reading the MCNP output file. Table 1 below shows the selection of these powers for the plasma major radius $R_0 = 1$ m and a fusion power $P_{\rm tot} = 174$ MW. The main results are the total rate of energy deposition, $P_{\rm tot}$ and the rate of energy deposition, $P_{\rm cc}$ in the mid-plane zone $z = \pm 0.2$ m. The time for adiabatic heating within a defined temperature range $t_{\rm adi}$, and the cryogenic power $P_{\rm cryo}$ will be defined later.

Figure 3 shows plots of the natural logarithm of the heat deposition against the

Table 1. A selection of results (with external shield correction) for a plasma major radius $R_0 = 1.0\,\mathrm{m}$ and 174 MW fusion power as a function of superconducting core radius r_{sc} and shield thickness d. A small correction for the tungsten carbide external shield with water cooling has been made as detailed in section 4. The penultimate italic line shows the results that were used in the simplified Costley *et al* study with major radius $R_0 = 1.35\,\mathrm{m}$ also including the external shield. The bold italic line shows the results for the full Costley study including engineering features. The cryogenic power P_{cryo} will be defined in section 8 and the time t_{adi} for adiabatic heating constrained to a defined temperature rise in section 9.

r_{sc} (m)	d (m)	P_{cc} (kW)	P_{tot} (kW)	P_{cryo} (MW)	t_{adi} (s)
0.15	0.15	173.72	520.19	28.30	0.85
0.15	0.20	96.46	279.09	16.00	1.58
0.15	0.25	51.22	142.31	8.66	3.09
0.15	0.30	26.37	70.34	4.58	6.26
0.15	0.35	13.91	35.96	2.50	12.24
0.15	0.40	7.00	17.26	1.30	25.51
0.20	0.15	260.84	763.92	40.30	1.02
0.20	0.20	142.20	400.73	22.28	1.95
0.20	0.25	75.57	204.68	12.06	3.82
0.20	0.30	38.88	100.83	6.34	7.76
0.20	0.35	20.20	50.83	3.42	15.40
0.20	0.40	10.14	24.35	1.77	32.15
0.25	0.20	194.51	532.67	28.93	2.30
0.25	0.25	102.92	268.65	15.45	4.55
0.25	0.30	52.44	131.03	8.04	9.33
0.25	0.35	26.90	65.24	4.28	18.74
0.25	0.40	13.54	31.43	2.22	38.91
0.23	*0.37*	*7.85*	*29.80*	*1.66*	*88.00*
0.23	***0.32***	***13.72***	***56.40***	***2.98***	—

three variables of shield thickness, plasma major radius and superconducting core radius. The points fit rather well to the linear regression lines shown in all the plots. The slopes against any given variable are quite similar for all plots. Including fits to all the data points gives the mean slope against major radius $S_{R_0} = -1.276 \pm 0.070\,\mathrm{m}^{-1}$, the mean slope against superconducting core radius $S_{r_{\mathrm{sc}}} = 6.752 \pm 0.819\,\mathrm{m}^{-1}$ and the mean slope against shield thickness $S_d = -13.733 \pm 0.245\ \mathrm{m}^{-1}$. The good linearity means that a fair approximation to all the computed data can be obtained by choosing a median logarithm of heat deposition value at for example $(R_0, r_{\mathrm{sc}}, d) = (1.00\,\mathrm{m}, 0.2\,\mathrm{m}, 0.3\,\mathrm{m})$ and performing a linear summation of products of the distances from this point multiplied by the mean gradients:

$$\log_e P(R_0, r_{\mathrm{sc}}, d) = \log_e P(1.0, 0.2, 0.3) + (R_0 - 1.0)S_{R_0} + (r_{\mathrm{sc}} - 0.2)S_{r_{\mathrm{sc}}} + (d - 0.3)S_d\ . \quad (2)$$

As a test of the approximation, figure 4 shows the estimated natural logarithms of the 93 values of the heat depositions compared with their computed values. The

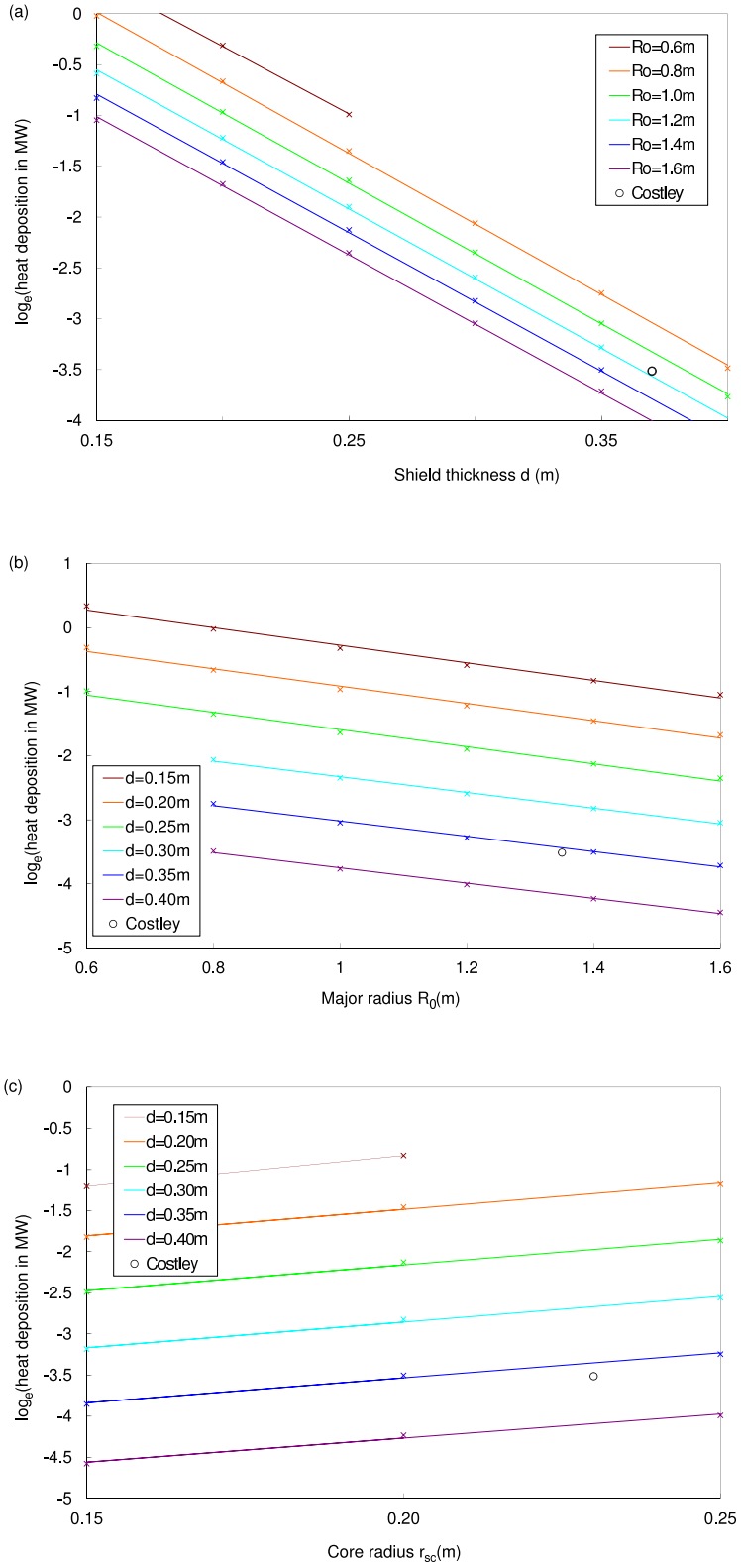

Figure 3. Three plots of the natural logarithm of the power deposition plotted against (a) the shield thickness d from plasmas at several major radii R_0 for a superconducting core radius $r_{\rm sc} = 0.2\,{\rm m}$, (b) the major radius R_0 for several shield thicknesses and (c) the superconducting core radius for a major radius of $R_0 = 1.4\,{\rm m}$. The lines are least squares fits to the data. The open circles indicate the Costley *et al* [2] pilot plant.

agreement has a standard deviation of 0.054 in the natural logarithm, or 5.5%.

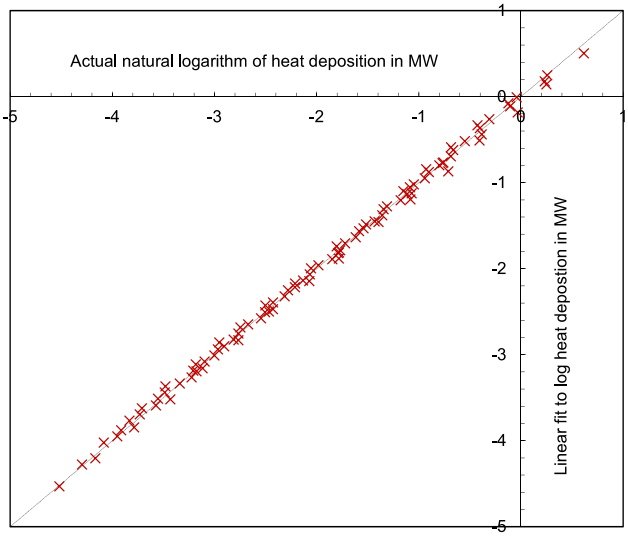

Figure 4. A scatter plot of the linear fit model for the logarithm of the heat deposition to the computed values.

Figure 5 illustrates some of the geometric factors that contribute to the results presented. Since the heat deposition from neutrons generated at any point at a radius R_0 will be the same, it is equivalent to view all neutrons as being generated at a single point at $(X,Y) = (R_0,\ 0)$ as indicated in the figure. All the distances involved in the calculation can be evaluated analytically [9]. A good fit of order 10% to the heat deposition computations at any given major radius could be made with the simple model that the neutrons travel through the shield and across the core along linear paths with an exponential attenuation depending on the material. The deposited power increases with core radius because of the increased solid angle, and decreases with shield thickness.

4. The effect of the plasma vessel outer surfaces

The previous section described results for the simplest situation of an elliptical cross-section plasma with shielding only of the central core containing the superconducting windings. All neutrons hitting the outer, upper and lower surfaces of the vessel were assumed lost. A subsequent calculation was performed for the situation with a 0.5 m cylindrical thick blanket shield starting at a radius of 1.55 m extending to 2.05 m, together with top and bottom surfaces also 0.5 m thick starting at $\pm$1.05 m and ending at $\pm$1.55 m. Figure 6 shows the layout of the shield including the various internal boundaries used to optimize the statistics in the MCNP calculation.

The results are given in table 2 below for the case of core radius $r_{\rm sc} = 0.2$ m and inner shield thickness $d = 0.4$ m. The computations with the external shield took considerably longer—around 20 hours. Looking first at the total power line of table 2, the power deposited into the central mid-plane region of the core for major radius

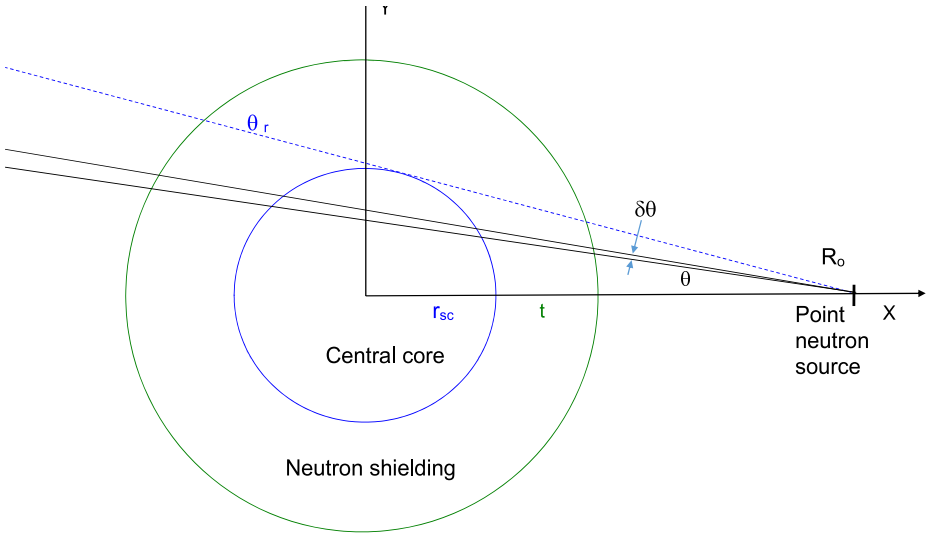

Figure 5. The geometric factors involved in the heat deposition into a shielded central superconducting core of radius r_{sc} surrounded by a cylindrical shield of thickness d from a neutron source at radius R_0. All the distances in the figure can be evaluated analytically and integrations made in the approximation of linear paths.

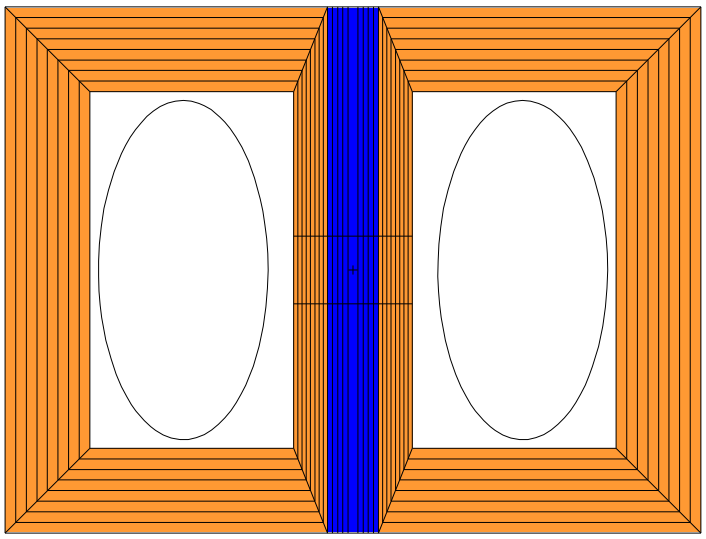

Figure 6. The inclusion of an external shield. The blue areas represent the central superconducting core, which now extends into the external shield. The orange shield surrounds the assembly at twice the thickness surrounding the core.

$R_0 = 1.0\,\mathrm{m}$, $r_{\mathrm{sc}} = 0.2\,\mathrm{m}$ and $d = 0.40\,\mathrm{m}$ has increased by about 6.5%. Looking at the mid-plane power, the inclusion of the external shield has increased the heat input by only 0.78%. It seems possible that the tungsten carbide and water outer shield appear rather "black" to the neutron flux and that relatively few are reflected back. Also, the spherical tokamak geometry means that the solid angle subtended by the central superconducting core at the outer wall is not large.

Table 2. The power deposition in kW of typical core and shield configurations without and with the external shields (outer, upper and lower) for a total fusion power of 174 MW and neutron power 139 MW.

	r_{sc} (m)	d (m)	No shield	With shield	Increase
Total deposited power P_{tot}	0.2	0.4	22.97 kW	24.46 kW	6.50%
Mid-plane deposited power P_{cc}	0.2	0.4	9.41 kW	9.48 kW	0.78%

5. The effect of the fusion neutron source profile

The first computations considered a small, uniform, elliptical cross-section neutron source centred near the major radius. It is known from both experiment and theory that the fusion neutron source profile is highly peaked within the perimeter of the plasma. This occurs because the neutron production varies as the square of the temperature. More precise profiles have been calculated using the SCENE [10] magneto-hydrodynamic (MHD) equilibrium code. The parameters used here were evaluated for a major radius $R_0 = 1.0\,\mathrm{m}$ and minor radius $a = 0.54\,\mathrm{m}$, with peaked density and temperature profiles. The number of fusion neutrons produced is given by $(N_{\mathrm{DT}}/2)^2\langle\sigma v\rangle$ where N_{DT} is the density of the deuterium-tritium fuel and $\langle\sigma v\rangle$ is the nuclear reactivity between D and T. Both the density and temperature are approximately constant on a flux surface, so the number of fusion-produced neutrons is also approximately constant on a flux surface. A fit to the equilibrium flux surfaces was made using the Miller [11] description in terms of the Shafranov shift, triangularity and elongation as a function of minor radius, and is given in table 3. The intensity of fusion-produced neutrons falls off exponentially with the minor radius; so that over 99% of the neutrons are produced within the first half of the minor radial distance and over 50% are generated within the first one-eighth.

Figure 7(a), on the left, shows the Miller poloidal flux surfaces at eight radial positions. However this profile is not straightforward to use with MCNP. Elliptical cross-section toroidal flux surfaces are standard in MCNP and the figure 7(b) on the right shows a similar set of flux surfaces using such elliptical toruses (which ignores the effects of triangularity). They differ appreciably near the top and bottom of the plasma but are very similar near the centre where most of the neutron intensity is concentrated. A choice has been made to centre each torus at the correct position determined by the Shafranov shift and to match the inner radius distance. This means that the radius

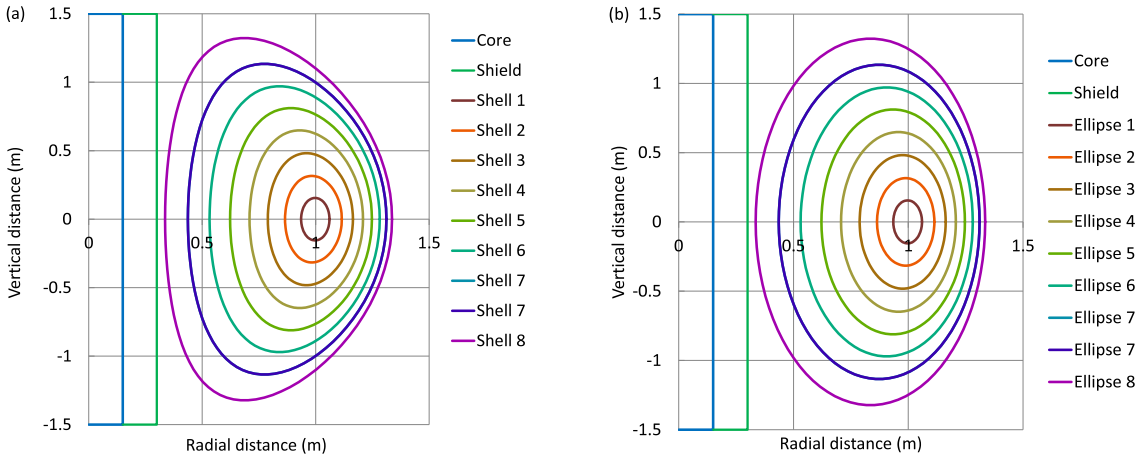

Figure 7. (a) The Miller [11] representation of the plasma flux surfaces for a plasma of major radius 1 m, superconducting core radius $r_{sc} = 0.15$ m, and shield thickness $d = 0.15$ m plasma. (b) By choosing elliptical cross sections with the same minimum radius as on the right, a very similar distribution is obtained, especially for the inner elliptical toruses which contain the bulk of the emission.

Table 3. The major radius R_0, radial minor radius a_r, vertical minor radius a_z and weight of the 8 radial shells.

Shell	R_0 (m)	a_r (m)	a_z (m)	Weight
1	0.9984	0.0625	0.1549	0.5321
2	0.9900	0.1250	0.3160	0.3358
3	0.9768	0.1875	0.4821	0.1080
4	0.9585	0.2500	0.6487	0.0258
5	0.9354	0.3125	0.8115	0.0057
6	0.9073	0.3750	0.9707	0.0013
7	0.8743	0.4375	1.1344	0.0003
8	0.8364	0.5000	1.3229	0.0001

at which the peak of the vertical height distribution occurs is in error, but this is only significant at larger minor radii where the emitted intensity is much lower. Using these elliptical toroidal flux surfaces it is possible to evaluate the heat deposition from each of the annular shells in turn, and to plot the heat deposition as a function of the shell number.

Figure 8 shows the total power deposited (circles) and the power deposited in the central 0.4 m of the central superconducting core (triangles) for each of the shells shown in figure 7(b) assuming that the same total power is emitted from each shell. One by one, the volumes between adjacent elliptical toruses are assumed to generate all the neutrons, so that it is possible to compare how the heat deposition varies. The point at "0" corresponds to all the emission taking place close to a ring at the major radius. It is seen that the total power increases as the shell number increases towards the outer boundary, while the power into the central region of the column decreases. However

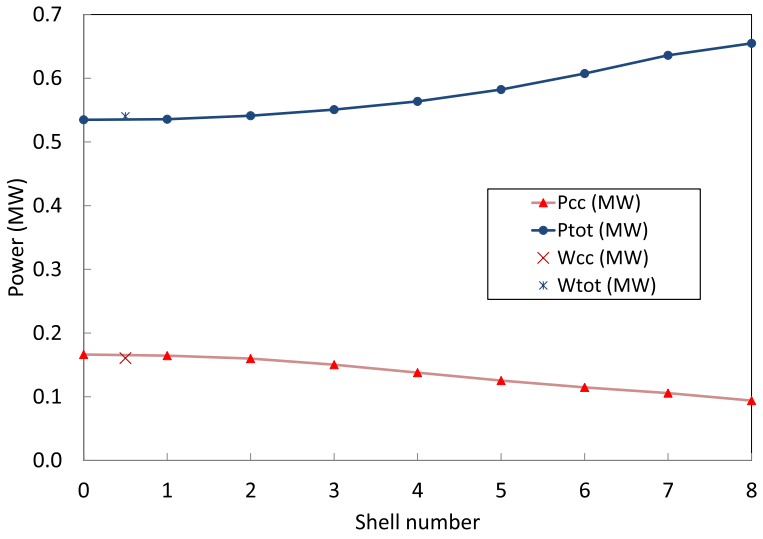

Figure 8. The heat deposition in MW into the full length of the superconducting magnet core region ($P_{\rm tot}$), and into the inner mid-plane 0.4 m high section ($P_{\rm cc}$). The full lines and points show the eight shells of increasing radii. The crosses $W_{\rm cc}$ and $W_{\rm tot}$ show the sums of these values weighted by their emission intensity. Note that, for this particular case of $R_0 = 1.0\,$m, $r_{\rm sc} = 0.15\,$m and $d = 0.15\,$m taking the central shell approximation underestimates the weighted full-length total deposited power by 2.3%. However, for the mid-plane region it is overestimated by 0.8%.

the changes become quite small when weighted according to a typical emission profile. The cross and plus signs indicate the heat deposition when an average of the eight shells weighted according to their intensity profile is taken. The weighted total heat deposition is within 1% of the emission from the first elliptical torus used in the earlier computations.

The set of toroidal shells may be used to evaluate the power deposition from any radial profile to within the approximation inherent in having only eight shells. As an example, figure 9 shows the averaged heat deposition as a function of the width constant in the exponential function describing the radial source profile. For low widths the averaged heat deposition approaches the same constant value as given by the line source. At high widths it again approaches a constant value close to that given by the outer shells. However the variation between these two limits is only about 15% so the effects of profile shape are not very large.

6. The choice of shield material

Several possibilities for the choice of shielding material were considered. Table 4 below shows the summary of results for the case of 0.15 m core radius, shielding thickness 0.15 m and major radius of 1 m with a fusion power of 174 MW. The table shows the neutron mean free path given by MCNP and the total deposited power.

Ignoring the shield and replacing it by a void has been suggested, reasoning that

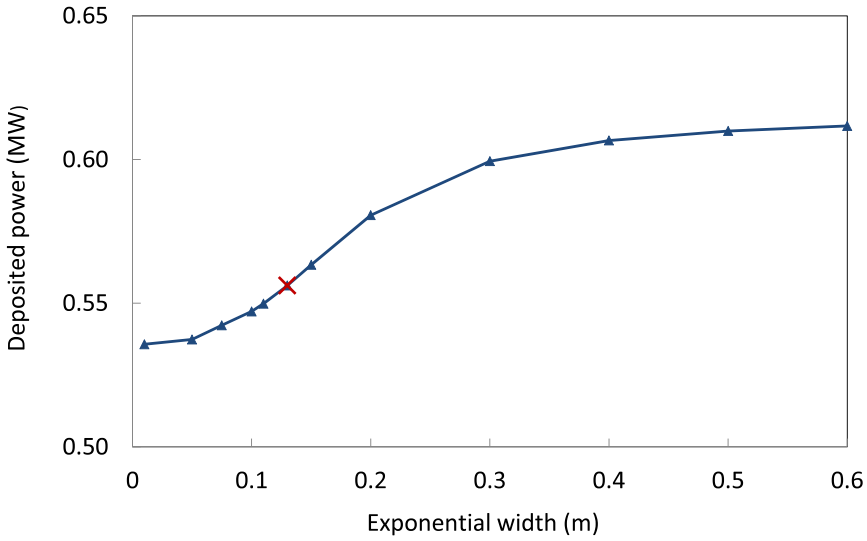

Figure 9. The total deposited power $P_{\rm tot}$ in MW as a function of the width of the exponential profile function for the same conditions as figure 8. The cross marks the width used in the other computations.

Table 4. The neutron mean free path and the total deposited power in the central superconducting core for the case of core radius $r_{\rm sc} = 0.15\,{\rm m}$ shield thickness $d = 0.15\,{\rm m}$, major radius $R_0 = 1\,{\rm m}$ and fusion power 174 MW.

Material	Average density ($\rm gcm^{-3}$)	Mean free path (mm)	Deposited power (MW)
Void shield	0.00	∞	2.13
Water-only shield	1.00	31	1.67
Hydrocarbon, CH_2	0.80	23	1.35
MnI_2, EuI_2 mixture	5.26	64	1.23
Zirconium borohydride, $Zr(BH_4)_4$	1.18	48	1.10
Tungsten carbide and water	11.83	19	0.49

the very fast 14.1 MeV neutrons have a fairly long mean free path (about 34 mm) in the largely copper core region and so will deposit little power. This is not confirmed. The copper region absorbs a considerable fraction of the power.

Similarly it has been suggested that a water or hydrocarbon shield (oil or polythene) will work by moderating the fast neutrons to thermal energies where they can be easily captured. The cross section of these materials is quite low in the slowing down MeV range, and thermalization hardly occurs. Water and hydrocarbons are good moderators but are poor at fast neutron shielding.

Cross section data suggest that elements with a large cross section in this slowing down region include manganese, europium and iodine. A 50% mixture by volume of europium iodide, EuI_2 and manganese iodide, MnI_2 was tried but the mean free path remains long and the power deposition in the central column high. Better performance was obtained with zirconium borohydride, $Zr(BH_4)_4$.

The last combination tried was a mixture of 66% tungsten carbide, 7.2% iron and 1.8% nickel with 25% cooling water. This gave the shortest mean free path and the best fusion power absorption of all the materials tried. The high atomic number of tungsten (74), its many absorption resonances in the keV range and the high density of tungsten carbide ($15.63\,\mathrm{gcm}^{-3}$) are likely to be the key to its good performance. This material has also been noted by Hong *et al* [12] as the best material for neutron shielding from the variety of materials they considered.

7. Interpolation between the corrected results using linear least squares fitting

The computations presented in section 3 have been approximately corrected for the effect of the outer shield discussed in section 4 and for the use of one elliptical torus rather than a weighted sum discussed in section 5 and fitted to a more precise linear interpolation than that given in (2). For arbitrary values of the parameters (R_0, r_{sc}, d), first the nearest of the computed array points (R_{0_i}, r_{sc_i},d_i) is found. A linear interpolation is then made, similar to that of (2) but using local values for the gradients with respect to R_0, r_{sc} and d and starting from the nearest computed point. The reliability of these fits can be found by dividing the dataset of computed values into a 50% training and 50% testing set, and using the training set for performing the linear interpolation constants, and comparing the interpolated values at the test points with their actual values. A scatter plot of the predicted logarithm of the heat deposition against actual values is shown in figure 10. The test points fit to the computed values to within 2.2%. This procedure was written into a Visual Basic macro, which has been incorporated into the systems code described by Costley *et al* [2].

8. The cryogenic power needed to remove the calculated heat load

The heat deposition into the superconducting central core of any power plant will have to be removed actively by, for example, liquid neon, as assumed in the computations, or more conventionally by cold helium gas from a cryoplant. Computation shows that for the 1.35 m major radius pilot plant the heat deposition increases by 12.4% when helium gas is substituted for the neon liquid. An important factor in any plant optimization will be the electrical power needed to run the cryoplant. Two important parameters in this calculation are the desired temperature of the superconducting core T_{cold}, say 20 K, and the temperature of the hot cooler into which the heat will be dumped T_{hot}, say 300 K. The Carnot coefficient of performance, CoP is the maximum efficiency possible in such a process and is given by $CoP = T_{\mathrm{cold}}/(T_{\mathrm{hot}} - T_{\mathrm{cold}})$

The Carnot coefficient of performance must be multiplied by the practical efficiency of any given cryoplant. Strobridge in 1974 collected together many of the efficiency measurements made at that time [13]. A clear result, which has not been altered by more recent data, is that the efficiency depends mostly on the capacity of the cryogenic

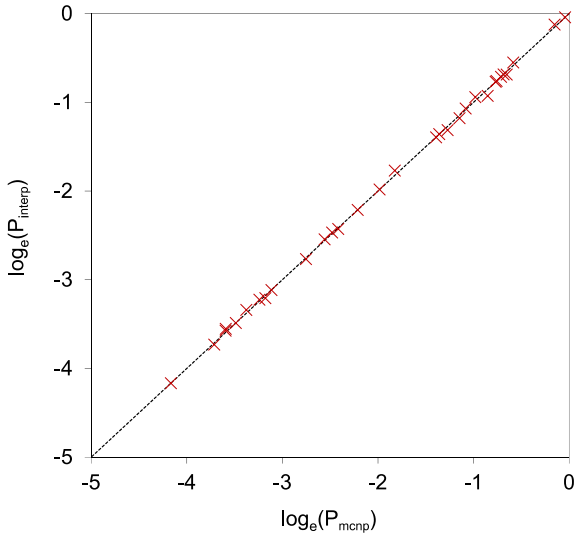

Figure 10. A scatter plot of the interpolated natural logarithms $\log_e P_{\rm interp}$ of the power deposition compared with those computed using the MCNP code $\log_e P_{\rm mcnp}$. The differences are only about 2%.

unit and not particularly on the temperature difference. His results can be well fitted by the line $\eta_{\rm practical} = (6.5 \log_{10} E + 16)\%$ where E is the deposition power in kW. The overall efficiency $\eta_{\rm l} = CoP\eta_{\rm practical}$ will be the product of the Carnot coefficient of performance and the practical efficiency. This number is also incorporated into the Costley *et al* system code.

As an example the pilot plant considered by Costley *et al* with major radius $R_0 = 1.35\,{\rm m}$, core radius $r_{\rm sc} = 0.23\,{\rm m}$ and shield thickness $d = 0.37\,{\rm m}$ has a heat deposition of 29 kW. Using the results from the system code with these parameters it is seen that the Carnot efficiency with the conductors at 20 K and the heat sink at 320 K is 0.066. The Strobridge efficiency for 29 kW is 0.265 so the overall efficiency is 1.77%, and the cryogenic power requirement is 1.66 MW.

9. The adiabatic rate of temperature rise in a superconducting core

In some experimental pilot power plants, it may not be necessary to remove all the heat deposited into the central superconducting core at the rate at which it is delivered. Rather, for short experiments with pulse lengths of the order of the current equilibration time, typically ten times the plasma energy confinement time, it may be possible to use the thermal inertia of the large mass of the core to limit the temperature rise during the experimental period to an acceptable value. In addition there are also the plasma build-up and ramp-down times lasting another ten or so confinement times, during which there will be some power deposition. For conventional low-temperature superconductors even a modest temperature rise of say 10 degrees is likely to be unacceptable, but this is no longer true for high-temperature superconductors which can be cooled to many degrees

below their transition temperature. The key parameters are the mass of the core, the initial temperature T_i of the superconducting core, the final temperature T_f which the core can be allowed to rise to, and the specific heat C_v of the core material around the temperature of interest. For this calculation, the core material is likely to be mostly copper with stainless steel strengthening and cladding. Figure 11 shows the specific heats of 316 stainless steel and OFCH copper as a function of temperature [14].

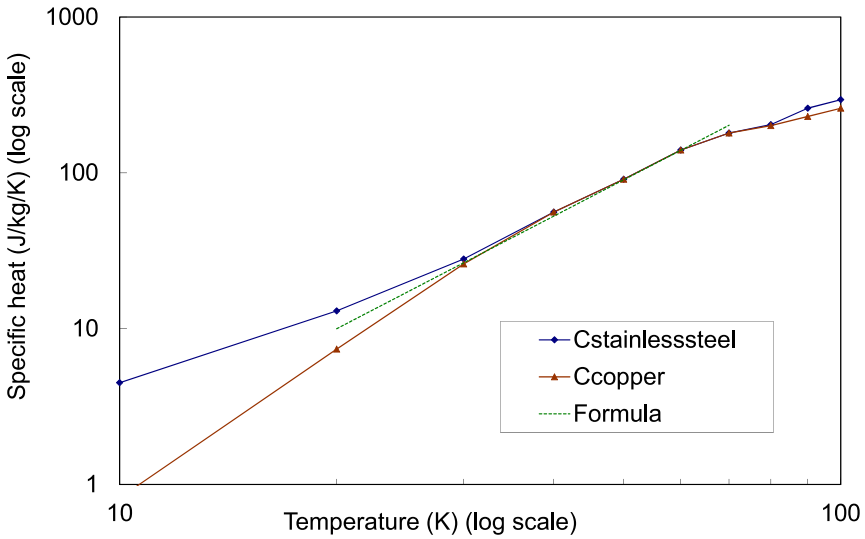

Figure 11. The specific heat of 316 stainless steel and copper over the temperature range from 10 K to 100 K. On this log-log plot the curves in the region relevant for high temperature superconductors, say 20 K to 60 K are almost identical and can be adequately fitted by the power law $C_\mathrm{v} = C_0(T/T_\mathrm{i})^p$

.

It is seen that in the important temperature range of between 20 K and 60 K they are very similar and follow roughly a power law curve $C_\mathrm{v} = C_0(T/T_\mathrm{i})^p$ where $C_0 = 10\,\mathrm{Jkg^{-1}K^{-1}}$, $T_\mathrm{i} = 20\,\mathrm{K}$ and $p = 2.4$. This line is shown by the dotted curve in figure 11.

In a demonstration experiment, steady-state pulses at full power are not foreseen but the pulse duration should be long enough that a stable plasma exists for at least a few plasma confinement times. The relevant time for establishing steady-state plasma conditions is the current equilibration time, which is typically 10 to 20 times the energy confinement time. In this case the heat deposition may be much larger than the cryogenic cooling rate so that the process is essentially adiabatic; there is negligible time for further cooling or heat loss by conduction, and all the deposited heat is used in raising the temperature of the central core. Suppose also that the temperature of the superconducting core is initially at $T_\mathrm{i} = 20\,\mathrm{K}$ and will be allowed to rise to say $T_f = 30\,\mathrm{K}$ during the experiment. During a short time Δt the temperature T will rise by a small increment ΔT given by

$$\Delta T = P_\mathrm{tot}\Delta t/(C_\mathrm{v}M) \tag{3}$$

where $C_{\rm v}$ is the specific heat in $\mathrm{JK^{-1}kg^{-1}}$, $P_{\rm tot}$ is the power level in watts and M is the mass in kg. The time interval $t_{\rm adi}$ during which the temperature rises from $T_{\rm i}$ to $T_{\rm f}$ is the integral

$$\begin{aligned} t_{\rm adi} &= \frac{M}{P_{\rm tot}} \int_{T_{\rm i}}^{T_{\rm f}} C_{\rm v}(T)\,{\rm d}T \\ &= \frac{M}{P_{\rm tot}} \int_{T_{\rm i}}^{T_{\rm f}} C_0 (T/T_{\rm i})^p\,{\rm d}T \\ &= \frac{MC_0}{P_{\rm tot}T_{\rm i}^p}\left[T_{\rm f}^{p+1} - T_{\rm i}^{p+1}\right] \end{aligned} \tag{4}$$

It is thus proportional to the heat capacity constant C_0, the mass M of the central column and the difference of the $(p+1)^{th}$ powers of the upper and lower temperatures. It is inversely proportional to the p^{th} power of the starting temperature and the deposited power.

The last column in table 1 shows this time for a variety of conditions. This calculation has also been incorporated into the Costley *et al* systems spreadsheet. For their pilot plant conditions the time to increase the superconducting core temperature from 20 K to 30 K is 88 seconds, which corresponds to some 282 ITER scaling (98y2) confinement times. This time should be sufficient to enable an adiabatic experiment to be completed without difficulty.

10. Discussion

The heat deposition into the central superconducting core of radius $r_{\rm sc}$ of a tokamak of major radius R_0, with a shield of thickness d is presented over a wide range of these variables. For all three variables the heat deposition varies nearly exponentially over the ranges considered, so that interpolation can be carried out to within a 2% accuracy. The inclusion of an outer shield and the likely effects of plasma profile are shown not to have a major influence. Tungsten carbide with water cooling is shown to combine good neutron and gamma ray shielding properties because of its high density, atomic number and good moderating properties.

For the $R_0 = 1.35\,$m pilot plant considered by Costley *et al* [2] the heat deposition is 29 kW which could be removed by a 1.7 MW cryoplant. Alternatively, the comparatively large mass of the central core could enable an adiabatic experiment to be performed where a core temperature rise from 20 K to 30 K could take place over a time span of 88 seconds or 282 confinement times.

The application of our computations to a pilot plant optimization is illustrated in figure 12. This shows a series of output parameters from the Costley *et al* [2] system code as the plasma major radius is varied. The code assumes a central superconducting core of $r_{\rm sc} = 0.23\,$m for $R_0 = 1.35\,$m, scaling in proportion to R_0. The code then evaluates the core heat deposition $P_{\rm tot}$ by interpolation, and from this the cryogenic power $P_{\rm cryo}$ required. It is seen that even at $R_0 = 0.9\,$m the deposited power is less than 100 kW and the cryogenic power less than 5 MW. At still smaller plasma major radii, adiabatic

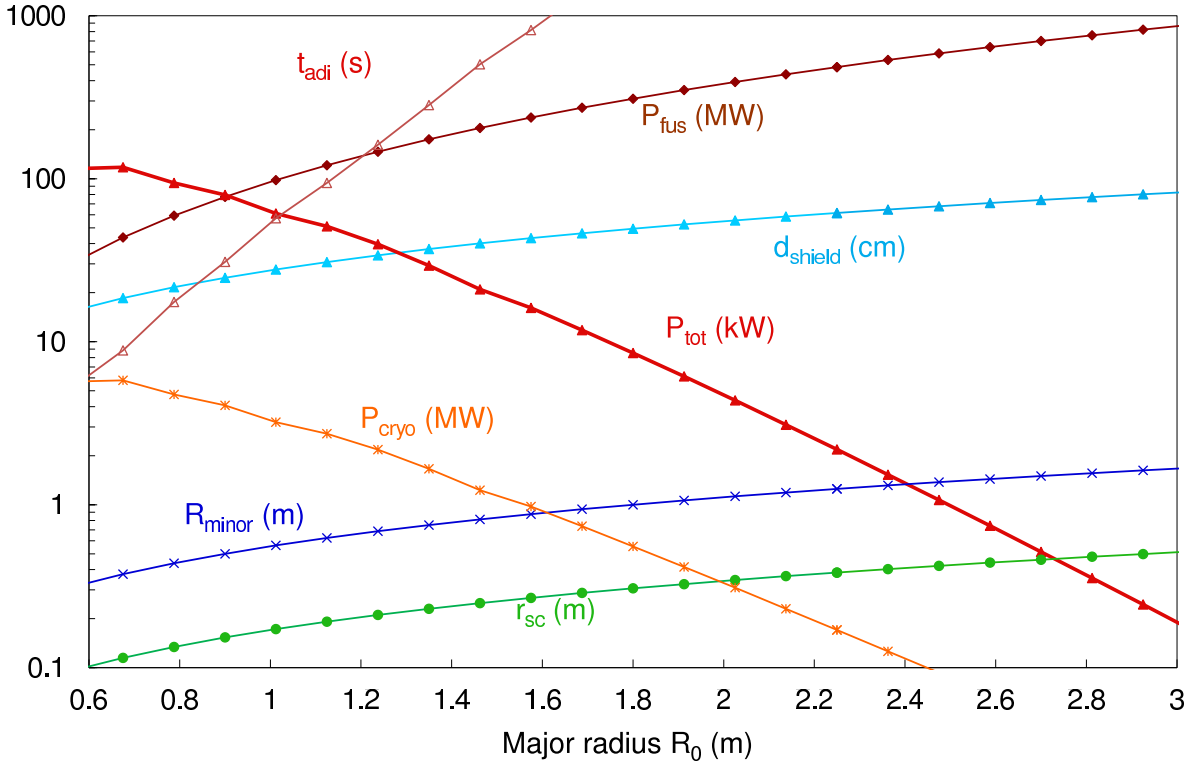

Figure 12. Examples of the use of the interpolated computations to investigate pilot fusion plants of differing major radii using the Costley *et al* system code [2]. The aspect ratio is fixed at 1.8 corresponding to spherical tokamaks and the toroidal field is fixed at 4 T. The system code is used to generate the other parameters. The curves show the fusion power $P_{\rm fus}$, the power into the superconducting core $P_{\rm tot}$, and the cryogenic power $P_{\rm cryo}$. Open symbols show the adiabatic time for a temperature rise from 20 K to 30 K.

experiments become attractive. For example at $R_0 = 0.6$ m, the larger superconducting core temperature rise from 20 K to 40 K takes 6.4 s or 54 ITER98 confinement times.

The effects of engineering features considered in the paper of Costley *et al* [2] such as a 0.05 m steel centre rod, 0.03 m thermal shield and 0.05 m plasma-wall gap have been investigated and they result in a significant 89% increase in the heat deposition. They continue to be studied individually to assess their relative importance and are being included into the system code.

Acknowledgments

The authors are grateful to many colleagues, especially Alan Costley, Mikhail Gryaznevich, Zach Hartwig, David Kingham, George Smith, Alan Sykes, Dennis Whyte and Martin Wilson for many helpful discussions.

References

[1] Sykes A, Gryaznevich M P, Kingham D, Costley A E, Hugill J, Smith G, Buxton P, Ball S, Chappell S, and Melhem Z. Recent advances on the spherical tokamak route to fusion power. *IEEE Transactions on Plasma Science*, **42**(3):482–8, March 2014.

[2] Costley A E, Hugill J, and Buxton P. New findings on the power and size of tokamak fusion pilot plants and reactors that potentially lead to smaller devices. *(Submitted to Nuclear Fusion)*, 2014.

[3] Stambaugh R D, Chan V S, Garofalo A M, Sawan M, Humphreys D A, Lao L L, Leuer J A, Petrie T W, Prater R, Snyder P B, Smith J P, and Wong C P C. Fusion nuclear science facility candidates. *Fusion Science and Technology*, **59**(2):279–307, February 2011.

[4] Hartwig Z S, Haakonsen C B, Mumgaard R T, and Bromberg L. An initial study of demountable high-temperature superconducting toroidal field magnets for the Vulcan tokamak conceptual design. *Fus. Eng. and Design*, **87**(3):201–14, March 2012.

[5] El-Guebaly L A and The ARIES Team. ARIES-ST nuclear analysis and shield design. *Fus. Eng. and Design*, **65**(2):263–84, February 2003.

[6] Shultis J K and Faw R E. An MCNP primer. Technical report, Kansas State University, Manhattan, 2011. http://mne.ksu.edu/∼jks/MCNPprmr.pdf.

[7] A general monte carlo N-particle (MCNP) transport code. https://mcnp.lanl.gov/.

[8] Eisterer M. High fluence neutron irradiation of coated conductors. Keynote lecture: Workshop on Radiation Effects in Superconducting Magnets and Materials 2014, Wroclaw, Poland https://indico.fnal.gov/getFile.py/access?sessionId=40&resId=0&materialId=1&confId=7702, May 2014.

[9] Windsor C G. A linear path approximation for the pilot plant neutron shield. Unpublished report, February 2014.

[10] Wilson H R. SCENE—simulation of self-consistent equilibria with neoclassical effects. Technical Report FUS-271, UK Atomic Energy Authority, 1994.

[11] Miller R L, Chu M S, Greene J M, Lin-Liu Y R, and Waltz R E. Noncircular, finite aspect ratio, local equilibrium model. *Phys. Plasmas*, **5**(4):973–8, 1998. http://www.frc.gatech.edu/rotation2/millerequilibriumpop.pdf.

[12] Hong B G, Hwang Y S, Kang J S, Lee D W, Joo H G, and Ono M. Conceptual design study of a superconducting spherical tokamak reactor with a self-consistent system analysis code. *Nucl. Fusion*, 51(11):113013, November 2011.

[13] Strobridge T R. Cryogenic refrigerators, an updated survey. Technical Report Tech. Note 655, National Bureau of Standards, 1974.

[14] Marquardt E D, Le J P, and Radebaugh R. Cryogenic material properties database. In *11th Int. Cryocooler Conf.*, pages 681–7. National Institute of Standards and Technology, Springer, June 2002. http://cryogenics.nist.gov/Papers/Cryo_Materials.pdf.